

Formation of Transient Coronal Holes during Eruption of a Quiescent Filament and its Overlying Sigmoid *

Li-Heng Yang^{1,2}, Yun-Chun Jiang¹ and Dong-Bai Ren^{1,2}

¹ National Astronomical Observatories/Yunnan Observatory, Chinese Academy of Sciences, Kunming 650011; yangliheng@ynao.ac.cn

² Graduate school of Chinese Academy of Sciences, Beijing 100049

Abstract By using $H\alpha$, He I 10830, EUV and soft X-ray (SXR) data, we examined a filament eruption that occurred on a quiet-sun region near the center of the solar disk on 2006 January 12, which disturbed a sigmoid overlying the filament channel observed by the *GOES-12* SXR Imager (SXI), and led to the eruption of the sigmoid. The event was associated with a partial halo coronal mass ejection (CME) observed by the Large Angle and Spectrometric Coronagraphs (LASCO) on board the Solar and Heliospheric Observatory (*SOHO*), and resulted in the formation of two flare-like ribbons, post-eruption coronal loops, and two transient coronal holes (TCHs), but there were no significantly recorded *GOES* or $H\alpha$ flares corresponding to the eruption. The two TCHs were dominated by opposite magnetic polarities and were located on the two ends of the eruptive sigmoid. They showed similar locations and shapes in He I 10830, EUV and SXR observations. During the early eruption phase, brightenings first appeared on the locations of the two subsequent TCHs, which could be clearly identified on He I 10830, EUV and SXR images. This eruption event could be explained by the magnetic flux rope model, and the two TCHs were likely to be the feet of the flux rope.

Key words: Sun: filaments — Sun: chromosphere — Sun: coronal mass ejections (CMEs)

1 INTRODUCTION

Coronal mass ejections (CMEs) are sudden eruptions of magnetized plasma from the solar corona into the heliosphere that can represent a large-scale rearrangement of the coronal magnetic field. CMEs have been considered to be the cause of interplanetary shocks and the driver of geomagnetic storms. In particular, halo CMEs have a great influence on space weather, because they may be directed earthward and so can lead to significant geo-disturbances (Jing et al. 2004). Although the halo CMEs have been extensively investigated, their origin and initiation are still not well understood. Therefore, identifying the on-disk CME signatures is vital for detecting earth-directed CMEs and for an understanding of the ultimate driving mechanism of CMEs, as well as for the forecast of space weather. Various warning signs of CMEs have been identified by in recent work, such as flares, eruptions of filaments and sigmoidal structures, transient coronal holes (TCHs), and so on (Hudson & Cliver 2001). However, the relationship between the on-disk surface activities and CMEs needs to be further checked. In a few CME events, very weak surface activities led to an earthward CME. For example, the event on 1997 January 6 showed that a very weak and unimpressive solar activity induced a halo CME and a geomagnetic storm (Webb 1998). Another similar event reported by Jiang et al. (2006) showed that a filament eruption without associated $H\alpha$ and *GOES* flare was related to a partial halo CME. These weak surface activities are significant to predict the space weather, and so cannot be ignored.

* Supported by the National Natural Science Foundation of China.

TCHs have been identified as key on-disk indicators of CMEs in some halo events with observations from *Yohkoh* Soft X-ray (SXR) Telescope and the Extreme Ultraviolet Imaging Telescope (EIT) on board the *Solar and Heliospheric Observatory (SOHO)* (Thompson et al. 1998; Wang et al. 2000). It has been found that they are often associated with eruptions of filaments or sigmoidal structures (Sterling et al. 2000; Jiang et al. 2007b), and appear as darkenings in SXR and EUV and brightenings in He I 10830 Å (Toma et al. 2005) in regions of unipolar opening magnetic field, with lifetimes of about a few hours to days generally, and can give rise to transient high-speed wind (Rust 1983).

Since their typical timescale of formation is less than an hour, much shorter than the typical radiative cooling timescale of about 36 hours in the corona (Hudson et al. 1996), the TCHs are often interpreted as due to density depletions, rather than temperature variation. A pair of compact and symmetric TCHs dominated by opposite polarities can form immediately close to the two ends of an eruptive filament or, sometimes, a sigmoid. It is believed that they mark the positions of the footpoints of the flux rope and the mass loss from them is expelled into the CMEs (Sterling & Hudson 1997; Webb et al. 2000; jiang et al. 2006).

Moreover, such dual TCHs can have $H\alpha$ counterparts, which means that they could extend from the corona deep into the chromosphere (Jiang et al. 2003). More recently, Toma et al.(2005) and Jiang et al.(2007a) found that some twin TCHs showed up above a clear chromospheric network pattern consisting of patchy bright/dark $H\alpha$ /He I 10830 Å plages with strongly concentrated magnetic network elements, as darkenings/brightenings of these plages during eruptions of the associated filament. It was further found that these TCHs were often preceded by chromospheric and coronal brightenings in the rising phase of the associated flares. Up to now, however, only a few such cases were observed, and the cause and role of the plages and preceding brightenings in the formation of TCHs are still not clear. To understand clearly the relationship of the brightenings and the following TCHs, and the eruption process and the associated CMEs, further observations are strongly needed.

In this paper, we present multi-wavelength observations of the eruption of an S-shaped filament that occurred on 2006 January 12, in which twin TCHs were formed in He I 10830 Å, EUV, and SXR. This eruption was not associated with any recorded *GOES* or $H\alpha$ flare but was directly related to a partial halo CME observed by the Large Angle and Spectrometric Coronagraphs (LASCO) on board *SOHO*. We will show that the brightenings clearly appeared at the locations of the following TCHs and the TCHs were possibly part of the on-disk proxy of the CME source region.

2 OBSERVATIONS

For the present work, the following data are used:

- 1 Full-disk He I 10830 Å intensity and velocity images from the Chromospheric Helium Imaging Photometer (CHIP, MacQueen et al. 1998) and $H\alpha$ disk images from the Polarimeter for Inner Coronal Studies (PICS) at the Mauna Loa Solar Observatory (MLSO). The CHIP data were acquired using a tunable Lyot filter (≈ 0.13 bandpass) positioned at seven wavelengths covering the spectral region from 10826 to 10834 Å, which provides a measure of the line-of-sight velocity of a filament over 100 km s^{-1} . The cadence of these images is 3 minutes and the pixel size is $2.3''$. The PICS disk images were acquired by using a narrowband filter of $\pm 0.5 \text{ Å}$ which allows for line-of-sight velocities about $40\text{--}45 \text{ km s}^{-1}$. These images have the same cadence with the CHIP data and a resolution of $2.9'' \text{ pixel}^{-1}$ (Toma et al. 2005).

2. Full-disk EUV images from the EIT (Delaboudinière 1995) on *SOHO*. EIT images are taken in four spectral bands centered on Fe IX/X (171 Å), Fe XII (195 Å), Fe XV (284 Å), He II (304 Å), which allow imaging of the solar plasma at temperatures ranging from $6 \times 10^4 \text{ K}$ to $3 \times 10^6 \text{ K}$. For the present work, the EIT provided 195 Å images with cadence of 12 minutes and pixel size of $2.6''$, while the 304 Å and 284 Å images were taken only once every 6 hours.

3. Full-disk SXR images from the *GOES-12* Solar X-ray Imager (SXI, Hill et al. 2005). For the current work, SXR images were taken every two minutes using thin polyimide filter. These images cover a wavelength range of 0.6–60 nm (sensitive to the temperature of 0.9–20 MK), at a pixel size of $5''$.

4. Full-disk longitudinal magnetograms from the Michelson Doppler Imager (MDI, Scherrer et al. 1995) on *SOHO*, with cadence of 96 minutes and pixel size about $2''$.

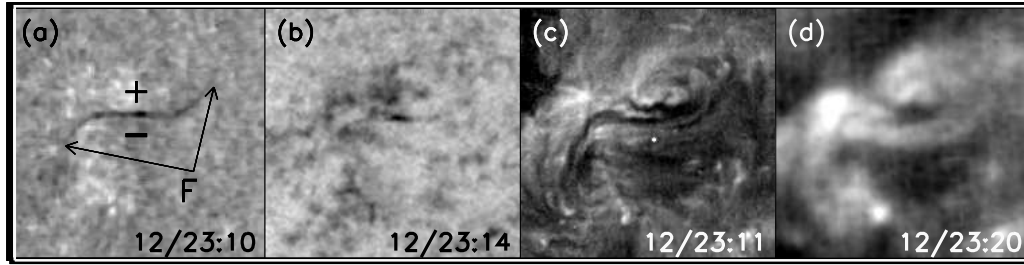


Fig. 1 MLSO/PICS $H\alpha$ line center (a), MLSO/CHIP He I 10830 Å intensity (b), EIT 195 Å (c), and SXR SXR (d), showing the appearance of the filament, “F”, before its eruption. The field of view (FOV) is $475'' \times 475''$.

5. C2 and C3 white-light coronagraph data from LASCO, which cover the range of 2 to 6 and 4 to 32 solar radii, respectively (Brueckner et al. 1995).

3 RESULTS

The eruptive filament, “F”, was located on a quiet-sun region in the southern hemisphere centered at S03W16, on January 12. Figure 1 shows the general appearance of the eruptive region before the F eruption in the $H\alpha$, He I 10830 Å, EIT 195 Å, and SXR images, respectively. In the $H\alpha$ image (Fig. 1a), F, indicated by the two black arrows, clearly shows an inverted S shape. As expected, it lies along a polarity inversion zone of the photospheric magnetic fields, and the corresponding positive/negative polarity on either side is marked by plus/minus sign. When F can be identified as a dark feature in He I 10830 Å (Fig. 1b), its EUV counterpart was clearly seen and showed a similar inverted S shape in the EIT 195 Å image (Fig. 1c). However, F in EUV appeared more complicated and bifurcated, and the same bifurcation was seen in the SXR image. In the higher temperature wavebands, F appeared increasingly broader. From SXR/SXR image (Fig. 1d), we also note an inverted S sigmoid located just above the F, indicating that they could belong to the same topological structure. This is consistent with the observation of Pevtsov (2002) that the chromospheric filament and the coronal sigmoid had a close spatial association. Although we can not determine F’s chirality from its barb orientations due to the poor spatial resolution of the $H\alpha$ observations, we conclude that the axial field of F before its eruption was directed eastward since the sign of the photospheric magnetic field in the F ends was negative in the southeast and positive in the northwest (see Fig. 3a). According to the definition given by Martin et al. (1994), F was dextral. However, it is noted that the chirality pattern consistent with both the dextral F and the inverted S sigmoid disobeyed the hemispheric chirality rule for Fs and sigmoids in the southern hemisphere (Zirker et al. 1997).

Figure 2 shows the evolution of the eruption in $H\alpha$, He I 10830 Å, EIT 195 Å, and SXR/SXR. The eruption showed up as a total disappearance of F in $H\alpha$. We see that its inverted S shape was clearly discernible at 23:16 UT, but parts of it became invisible at 23:25 UT, and the whole F disappeared at 23:37 UT. In the He I 10830 Å velocity observations, however, F mainly showed blueshift signature, clearly indicating that the disappearance was due to its eruption. We also note that the blueshift signature could be detected at 23:44 UT, lagging the complete disappearance of F in $H\alpha$ by 7 minutes. This possibly suggests that the erupting F was fast enough to be Doppler shifted out of the filter of the MLSO/PICS instrument but was still in the detectable range of the MLSO/CHIP instrument. In EIT 195 Å images, we see that the dark EUV counterpart of the $H\alpha$ F also showed a consistent eruptive process. As a distinct feature of the event, however, the SXR sigmoid was strongly disturbed during the eruption, and it appeared that the sigmoid also underwent an eruption, which was made manifest by the clear disappearance of some loops that contained it after the F eruption. Thus, this event involved the eruptions of both the F and the sigmoid. This is greatly different from the cases studied by Pevtsov (2002) and Jiang et al. (2007b), in which coronal sigmoids underwent activations and eruptions while the underlying $H\alpha$ filaments were left largely untouched. The F eruption was accompanied by the occurrence of two flare-like ribbons, “R1” and “R2”, in $H\alpha$, He I

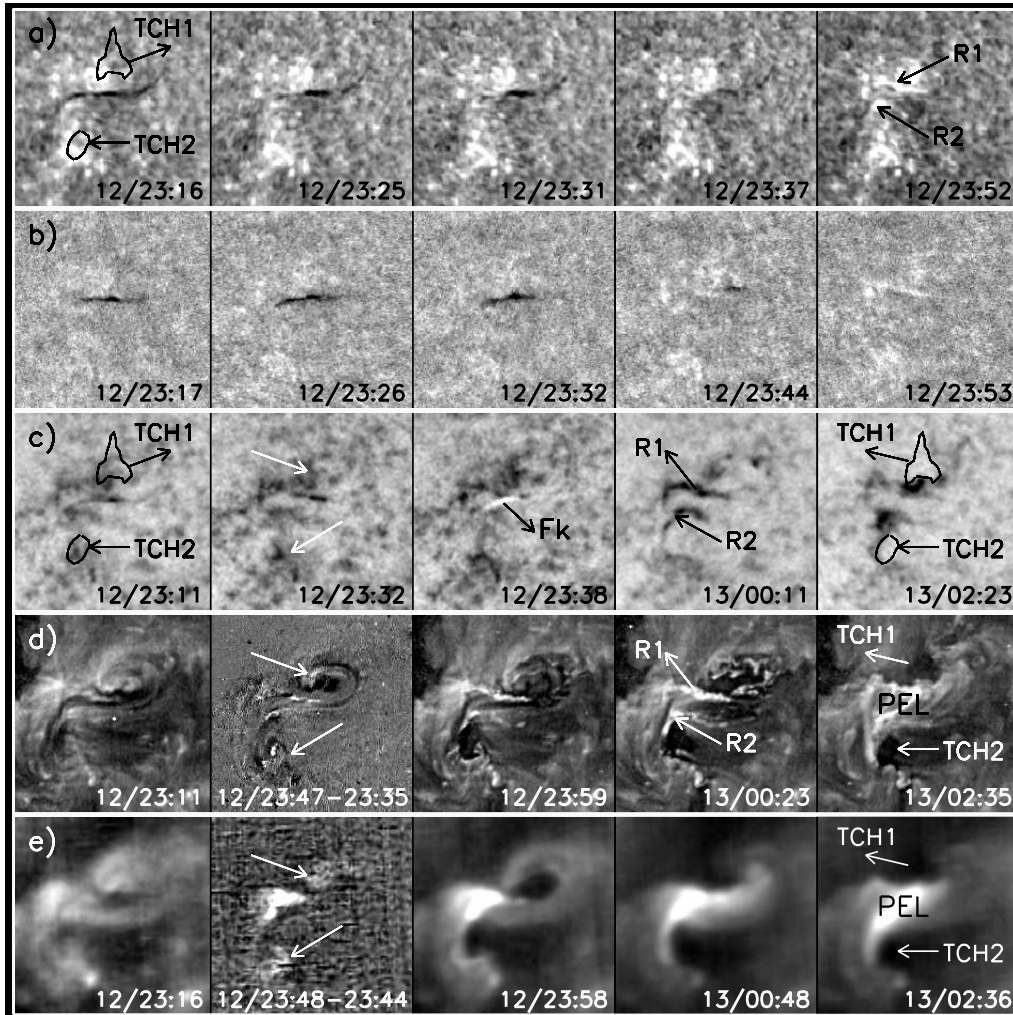


Fig. 2 MLSO/PICS $H\alpha$ line center (a), MLSO/CHIP He I 10830 Å velocity (b) and intensity (c), EIT 195 Å (d) and SXR (e), showing the evolution of the event. To clearly exhibit the brightenings in the early formation phase of the TCHs, a difference image is presented in the second column of (d)/(e). The FOV is the same as in Fig. 1.

10830 Å and EIT 195 Å lines. They were located on opposite sides of the eruptive F, and were dark in He I 10830 Å due to the increased absorption. Notably, a bright flare-like kernel, “Fk”, was visible from 23:35 to 23:44 UT in He I 10830 Å intensity images, this means that the energy release was large enough to change the He I 10830 Å absorption line into emission (Penn & Kuhn 1995).

After the F eruption, post-eruptive loops, “PELs”, gradually appeared in EUV and SXR observations. They connected the two flare-like ribbons, and their footprints expanded with the increasing separation of the ribbons. All of these observations indicated typical features of flares associated with F eruptions, but no optical flare was reported by the Solar Geophysical Data online around the time of the event. Furthermore, despite the *GOES* SXR flux showing an increase relative to the background level after the F eruption (see Fig. 5), no *GOES* flare above X-ray class B1 was recorded. Therefore, it seems that the flare-like ribbons were too weak to be regarded as an $H\alpha$ or *GOES* flare. As the SXR and $H\alpha$ wavebands each contain only

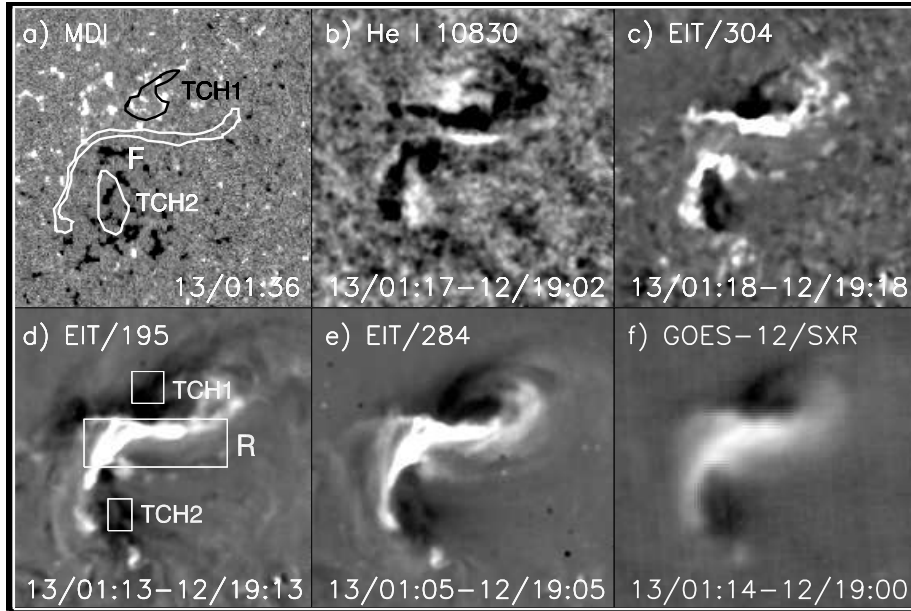


Fig. 3 MDI magnetogram (a), MLSO/CHIP He I 10830 Å (b), EIT 304 (c), 195 (d), and 284 Å (e), and SXI/SXR (f) difference images. The two TCHs, “TCH1” and “TCH2” are predominated by opposite polarities and are located on the two F ends. The TCHs and the pre-eruptive H α F are depicted by the black and white contours of (a). The FOV is the same as in Fig. 1.

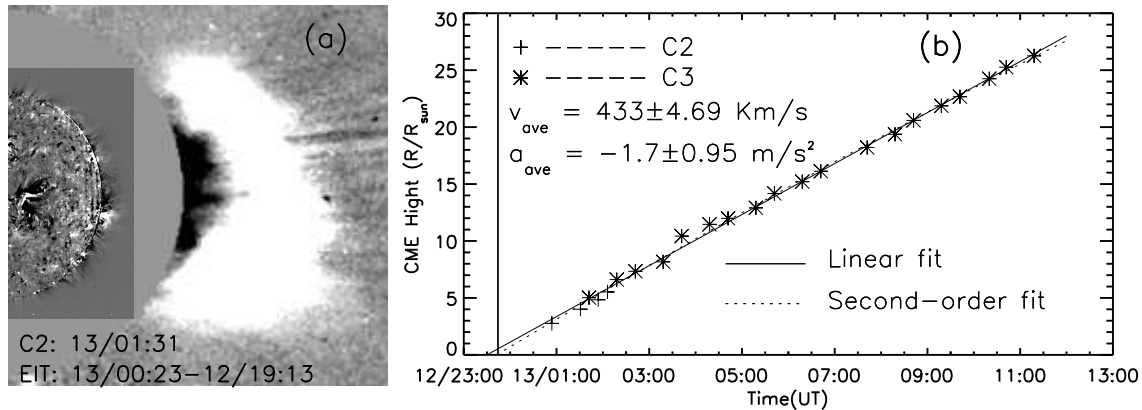


Fig. 4 (a) Composite image of the inner EIT 195 Å and the outer LASCO C2 difference images. (b) Height of the CME front as the function of time.

5–10% of the total radiated energy, it may not be proper to identify a flare with only these wavebands (Zhou et al. 2003). The EIT 195 Å light curve measured in the flare-like region is plotted in the Figure 5(a), and we note that the brightness increased about 125% from the starting time to the time of maximum enhancement. Due to the brightness at the start time was greater than that of the background, the enhancement could be considered as an EUV flare according to the criterion given by Zhou et al. (2003).

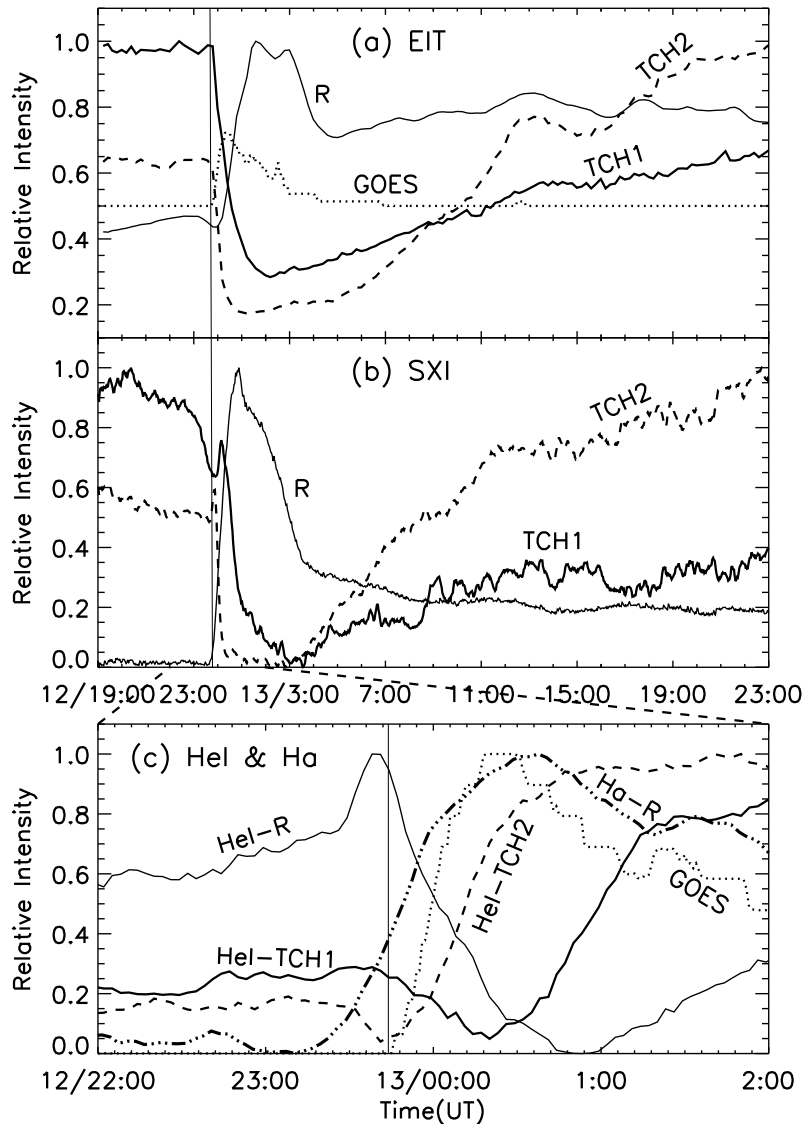


Fig. 5 Time profiles of *GOES-12/SXR* in the energy channel of 1–8 Å (dashed thin lines in Panels a and c), in arbitrary units and in units normalized to one, respectively. The light curves of EIT 195 Å (a), SXI/SXR (b), He I 10830 Å (c) intensities in areas centered on the TCH1, TCH2, and R (indicated by the boxes in Fig. 3(d)), and H α intensities (c) in an area centered on the R are computed from the intensity averaged over these regions. EIT 195 Å is normalized to the maximum value, and the SXI/SXR, He I 10830 Å and H α are normalized to one.

As another remarkable feature of the event, two TCHs, labelled “TCH1” and “TCH2”, were formed during the eruptions of the F and the sigmoid. After the eruptions, they were quite obvious in He I 10830 Å intensity, EIT 195 Å, and SXI/SXR images, see Figure 2. As in the cases investigated by jiang et al. (2003), Toma et al. (2005) and jiang et al. (2007a), it is noted that the dual TCHs were also preceded by faint brightenings in their early formation phase, which can be clearly seen in the He I 10830 Å intensity image, and the EVU and SXR difference images; see the second row of Figure 2 (indicated by the white arrows).

They were located at the sites of the following TCHs, and were kept away from the two flare-like ribbons, so were not the result of a spreading and expansion of these ribbons. Thus it appears that formation of TCHs is often associated with certain brightenings. Figure 3 shows the difference images from the pre-event images at He I 10830 Å, 304 Å, 195 Å, 284 Å and SXR/SXR lines. The TCHs, appearing as brightening regions in He I 10830 Å and dimming regions in EUV and SXR, had similar locations and shapes in these lines formed over a temperature range from several 10^4 K to 2×10^6 K, so indicating that they are caused by density depletions rather than by temperature variations (Thompson et al. 1998). Moreover, they occurred in opposite polarity regions near the two ends of the erupted sigmoid and flanked the central PEL.

A partial halo CME was observed by SOHO/LASCO around the time of the event. The CME was first detected by LASCO C2 at 00:54 UT on January 13, and later became visible in C3 at 02:42 UT located above the W limb. According to the measurements of Seiji Yashiro, its center position angle (PA) was 281° with a width of 126° . Figure 4a presents a composite image of an inner EIT 195 Å with an outer LASCO C2 difference image. We see that the eruptive region was nearly located along the direction of the central PA of the CME. The height-time (H-T) plot of the CME front at 267° is shown in Figure 4b. The average speed of the CME front given by a linear fitting was $433 \pm 4.96 \text{ km s}^{-1}$, and the average acceleration given by a second-order polynomial fitting was $-1.7 \pm 0.95 \text{ m s}^{-2}$ (shown in the upper left corner of Fig. 4b), indicating that the CME was a slow one, which is consistent with the results given by sheeley et al. (1999) that slow CMEs were often associated with filament eruptions. From the back extrapolation of the second-order polynomial fitting of the CME H-T plot to the solar disk center, we estimate that the onset time of the CME was about 23:45 UT on January 12 (marked by a vertical bar in Fig. 4 (b)), which was very close to the start time of the *GOES* 1-8 Å SXR flux increase and the onset time of the brightenings preceding the appearance of the two TCHs (marked by vertical bars in Fig. 5). These consistent spatial and temporal behaviors indicated that the F eruption and the two TCHs were directly related to the CME.

Figure 5 presents the profile of *GOES* 1-8 Å SXR flux and the light curves of EIT 195 Å, SXR/SXR, and He I 10830 Å intensities of the two TCHs and the flare-like regions and $H\alpha$ intensities of the flare-like region, respectively. Beginning at 23:45 UT on January 12 (marked by the vertical line in Fig. 5), the *GOES* SXR flux showed a weak increase, taking about 1 hour to reach the peak, which was below the X-ray class B1 level. So the enhancement was too weak to be recorded as a *GOES* flare. Furthermore, we see that EIT 195 Å, SXR/SXR light curves measured in the flare-like region are similar to the *GOES* 1-8 Å SXR flux profile, and the enhancement of the flare-like region began at about 23:45 UT, January 12. However, the start time of enhancement of the flare-like region in He I 10830 and $H\alpha$ light curves was earlier the time of disappearance of F. Especially, with the appearance of the flare-like kernel, the light curve showed an increase between 23:35 to 23:44 UT, January 12. We also note that during the formation of the two TCHs, the EIT 195 Å and SXR intensities obviously decreased and the He I 10830 Å intensity distinctly increased. In addition, we found that during the early eruption phase there was an increase in the SXR flux curves and a decrease in the He I 10830 Å flux curves due to the appearance of the brightenings, and the increase (decrease) lasted only during the rise phase of *GOES* 1-8 Å SXR flux curve.

4 CONCLUSIONS AND DISCUSSION

We have made an investigation on a filament eruption near the center of the solar disk on 2006 January 12, and on the associated brightenings, TCHs, and a halo CME, as well as the eruptive sigmoid above the filament. The main observational results are as follows: (1) The disappearance of the inverted S-shaped filament was followed by two flare-like ribbons, two TCHs, and post-eruption coronal loops, but no evident X-ray and $H\alpha$ flares were recorded. (2) During the early eruption phase, brightenings first appeared on the sites of the two TCHs, and were short lived during the rise phase of the flare, then the two TCHs were formed near the two ends of the sigmoid, dominated by opposite polarities, which were clearly visible in He I 10830 Å, EUV and SXR, with similar locations and shapes. (3) The partial halo CME showed a close spatial and temporal relation to the filament eruption and the two TCHs.

This event was not related to any recorded $H\alpha$ and *GOES* flares, while the usual feature of flares of two flaring ribbons, was identified in multi-wavelength observations ($H\alpha$, He I 10830 Å, EIT 195 Å), but it is hard to associate such a weak surface activity to the partial halo CME. Fortunately, the filament and the sigmoid eruption, and the formation of the two TCHs, which are considered to be predictors of the CME,

directed our attention to this event. It is incredible that such a very minor change in the chromosphere could bring about such a major coronal perturbation. Similar results have been obtained by Webb et al. (1998), and they found that some weak on-disk activities on 1997 January 6 led to a CME and the “problem” geomagnetic storms. Later, Shakhovskaya et al. (2002) showed that a prominence eruption on 2000 August 11 with no associated flares resulted in a faint CME. More recently, Jiang et al. (2006) reported a filament eruption on 1999 March 21 without flares recorded, which led to a partial halo CME. These events indicate that CMEs may or may not be related to flares in the chromosphere (Švestka 2001) and that weak events are valuable in identifying the source regions of the earth-directed CMEs, important for predicting space weather.

We have described a rare event where the eruptions of a quiescent filament and an overlying sigmoid led to the formation of the two TCHs, which is not related to any recorded flare events, which is very similar to the event of 1997 October 23 presented by Hudson and Cliver (2001). The $H\alpha$ filament and sigmoid are considered to be the signature of a flux rope system (Pevtsov 2002), and the eruption event can be explained by the flux model of CME, the two TCHs representing the two footprints of the flux rope (Sterling and Hudson 1997; Jiang et al. 2003; Jiang et al. 2006). However, during this event both the filament and the sigmoid erupted, unlike the observations by Pevtsov (2002) where the sigmoid activated and disappeared without a corresponding filament eruption.

According to the analytic 3-D MHD model of flux ropes proposed by Gibson and Low (2000), the two TCHs would appear anti-symmetrically on either side of the photospheric neutral line, and interpreted to be the counterpart of the CME cavity seen at the limb. The formation of the two TCHs could be explained by the opening of previous closed field lines or by the expansion of those related to the flux rope. The two TCHs clearly appeared on the 304 Å difference image, indicating that the feet of the flux rope were deeply rooted in the chromosphere, and that the mass loss may originate from the cooler and denser chromosphere. Meanwhile, the two TCHs had a temperature range from several 10^4 K to 2×10^6 K, suggesting that the appearance of the two TCHs was due to the density depletion rather than the temperature decrease. The mass loss probably provided a supplement to the CME. In addition, the brightenings appeared on the locations of the two TCHs at the initial phase of the flare, and their appearance may be the result of a flux rope eruption (Jiang et al. 2007a). This has not been described by any theoretical models, and further observational and theoretical investigations are needed for further understanding.

Acknowledgements The authors thank an anonymous referee for valuable comments. The $H\alpha$ and He I 10830 Å data are provided by the High Altitude Observatory, which is part of the National Center for Atmospheric Research under sponsorship of the National Science Foundation. The authors are indebted to the *SOHO*/EIT, MDI and LASCO teams, *GOES*/SXI team for free access to the wonderful data. This work is supported by the NSFC under grants 10573033 and 40636031, and by the 973 program (2006CB806303).

References

- Brueckner G. E., Howard R. A., Koomen M. J. et al., 1995, *Sol. Phys.*, 162, 357
 Delaboudinière J. P., Artzner G. E., Brunaud J. et al., 1995, *Sol. Phys.*, 162, 291
 Gibson S. E., Low B. C., 2000, *J. Geophys. Res.*, 105, 18187
 Hill S. M., Pizzo V. J., Balch C. C. et al., 2005, *Sol. Phys.*, 226, 255
 Hudson H. S., Acton L. W., Freeland S. L., 1996, *ApJ*, 470, 629
 Hudson H. S., Cliver E. W., 2001, *J. Geophys. Res.*, 106, 25199
 Jiang Y. C., Ji H. S., Wang H. M., Chen H. D., 2003, *ApJ*, 597, L161
 Jiang Y. C., Li L. P., Yang L. H., 2006, *Chin. J. Astron. Astrophys. (ChJAA)*, 3, 345
 Jiang Y. C., Yang L. H., Li K. J., Ren D. B., 2007a, *ApJ*, 662, L131
 Jiang Y. C., Chen H. D., Shen Y. D., Yang L. H., Li K. J., 2007b, *Sol. Phys.*, 7, 129
 Jing J., Yurchyshyn V. B., Yang G., Xu Y., Wang H. M., 2004, *ApJ*, 614, 1054
 MacQueen R. M., Blankner J. G., Elmore D. F., Lecinski A. R., White O. R., 1998, *Sol. Phys.*, 182, 97
 Martin S. F., Bilimoria R., Tracadas P. W., 1994, in R. Rutten and C. J. Schrijver (eds.), *Solar Surface Magnetism*, Kluwer Academic Publishers, Dordrecht, p. 303

- Penn M. J., Kuhn J. R. 1995, ApJ, 441, L51
- Pevtsov A. A., 2002, Sol. Phys., 207, 111
- Rust D. M., 1983, Space Sci. Rev., 34, 21
- Scherrer P. H., Bogart R. S., Bush R. I. et al., 1995, Sol. Phys., 162, 129
- Shakhovskaya A. N., Abramenko V. I., Yurchyshyn V. B., 2002, Sol. Phys., 207, 369
- Sheeley N. R., Walters, J. H., Wang Y.-M., Howard R. A., 1999, J. Geophys. Res., 104, 24739
- Sterling A. C., Hudson H. S., 1997, ApJ, 491, L55
- Sterling A. C., Hudson H. S., Thompson B. J., Zarro D. M., 2000, ApJ, 532, 628
- Švestka Z., 2001, Space. Sci. Rev., 95, 135
- Thompson B. J., Plunkett S. P., Gurman J. B., Newmark J. S., Cyr O. C. St., Michels D. J., 1998, Geophys. Res. Lett., 25, 2465
- Toma G. De, Holzer T. E., Burkepile J. T., Gilbert H. R., 2005, ApJ, 621, 1109
- Wang H. M., Goode P. R., Denker C., Yang G., Yurchishin V., Nitta N., Gurman J. B., Cyr C. St., Kosovichev A. G., 2000, ApJ, 536, 971
- Webb D. F., Cliver E. W., Gopalswamy N., Hudson H. S., Cyr O. C. St., 1998, Geophys. Res. Lett., 25, 2469
- Webb D. F., Cliver E. W., Crooker N. U., Cry O. C. St., Thompson B. J., 2000, J. Geophys. Res., 105, 7491
- Zhou G. P., Wang, J. X., Cao, Z. L., 2003, A&A, 397, 1057
- Zirker J. B., Harvey K., Gaizauskas V. 1997, Sol. Phys., 175, 27